Chapter 1

INTRODUCTION TO PHYSISORBED MONOLAYERS AND SCANNING TUNNELING MICROSCOPY

1.1 Physisorbed Monolayers

Many simple organic molecules, such as straight-chain alkanes, alcohols, and carboxylic acids, spontaneously assemble into highly ordered monolayers at solid–liquid interfaces. The first reports of this phenomenon were published in the scientific literature in the early 1960s when it was observed that organic molecules, in both neat liquids and in solution, form ordered monolayers on substrates such as graphite, cast iron, and molybdenum disulfide.[1,2] At the time, this discovery was primarily of interest to the lubrication and separation industries. The early studies of this phenomenon were conducted using microcalorimetry and consisted of measurements of the heat of adsorption or elution of alkanes and alcohols in contact with solids held at constant temperature. These early studies were typically conducted by injecting solutions of alkanes into a solvent stream flowing through an insulated cell containing a known amount of a powdered sample and measuring heat effects. The resulting data demonstrated that the alkanes formed monolayers on the surfaces of the solids and that the adsorption was due principally to intermolecular interactions such as van der Waals forces and hydrogen bonding rather than to strong interactions between the substrate and the adsorbed molecules.[3–7]

The heat of adsorption of long-chain alkanes onto cast iron was found to be linearly dependent upon the chain length and to increase negatively by ~ 2.5 kcal mol^{-1} for each carbon added to the chain; the measured heat effects increased with the carbon content of the cast iron.[1] This chain-length dependence is illustrated in Figure 1.1. The relationship between the measured heats of adsorption and the chain length of the molecules in the liquid indicates that intermolecular interactions such as van der Waals forces provide the driving force for the adsorption. Although interactions between the adsorbed alkanes and the surface are relatively weak compared to the intermolecular forces in the case of long-chain alkanes, interactions with the surface are important in the determination of whether physisorption will occur at all on a particular surface material. The heat of adsorption of *n*-dotriacontane was measured to be 36 kcal mol^{-1} for a graphite surface, but only 12 kcal mol^{-1} for a WS_2 surface, and 10 kcal mol^{-1} for a MoS_2 surface.[2] These data, combined with the tail on the plot shown in Figure 1.1 clearly demonstrate that a portion of the measured heats of adsorption is due to surface–adsorbate interactions. Interactions of this type, however, are dependent upon the fixed surface area of the adsorbate and are essentially independent of the length of the alkane chain. The potential for an adsorbate to form a monolayer structure somewhat commensurate with that of the surface and the polarizability of both the surface structure and the adsorbate molecules are likely to contribute to the strength of the surface–adsorbate forces.[8,9] These early studies also demonstrated that highly branched alkanes such as squalane would not form ordered monolayers.[10] The presence of branches sterically interferes with the intermolecular van der Waals interactions that drive physisorbed monolayer formation and can prevent the formation of an ordered monolayer.

The data obtained using calorimetry also allowed researchers to deduce the geometric structure of the molecular monolayer on a graphite surface. This was accomplished through a comparison of the measured surface area of the substrate with the number of molecules that became adsorbed to that substrate. These experimentally determined variables were then combined with the knowledge of the surface area that each adsorbed molecule would occupy in each possible spatial orientation. In this manner it was predicted that the long-chain normal hydrocarbons adsorbed to a graphite surface with their carbon skeletons lying parallel to the surface. It was also predicted that the carbon skeletons lie in registry with the graphite surface such that each methylene unit occupied one hexagon of the graphite basal plane, and such that the molecules were compressed by about 8–12% relative to their crystalline structures.[7]

The effect of varying the solvent was also examined using calorimetry, and it was observed that the monolayers formed more readily when dissolved in branched solvents than when dissolved in straight-chain solvents.[11,12]

The Parallel Layer Model was developed to explain the observed adsorption behavior. In this model, it is assumed that adsorbed molecules lie flat on the surface without tails extending into the bulk solution. Adsorption from solution is then treated as a heterogeneous displacement reaction between the solvent and the solute. The equilibrium expression can then be written as follows:

$$nX^{a} + Y^{l} = nX^{l} + Y^{a}$$

where *n* is the number of solvent molecules (*X*) replaced by a single solute molecule (*Y*). The superscripts *a* and *l* refer to the adsorbed and liquid phases, respectively.[13]

1.2 Scanning Tunneling Microscopy

In the early 1980s Gerd Binnig and Heinrich Rohrer of the IBM Research Division in Zurich introduced the scanning tunneling microscope (STM).[14–16] The revolutionary development of this instrument allowed relatively flat electrically conductive samples to be imaged with atomic resolution without contacting or otherwise disturbing the sample surface.

In scanning tunneling microscopy a very sharp metallic tip is scanned in a raster pattern above a conductive sample while a constant potential is maintained between the tip and the sample, as depicted in Figure 1.2. If the tip is sufficiently close to the sample surface a tunneling current will flow between the tip and surface. Electronic feedback controls in the instrument maintain either the height of the tip above the sample or the current between the tip and sample at a constant value. When the tip is maintained at a constant height, the current fluctuation is monitored and used to produce an image of the surface. If scanning is conducted by maintaining a constant current between the tip and sample, the fluctuation of the height of the tip over the sample is monitored and used to produce the surface image. Constant current mode imaging reduces the probability of accidental contact between the tip and surface, while constant height mode imaging permits the use of greater scan speeds. STM images always contain both topographic and electronic information about the sample surface.

The sensitivity of the STM is a product of the quantum mechanical tunneling effect which the method exploits. The magnitude of the tunneling current relates directly to the probability of an electron tunneling through a potential barrier present between the tip and surface, and essentially reduces to a particle-in-box problem. For a rectangular potential barrier, the solutions to this problem have the form $\Psi = e^{\pm \kappa z}$, with $\kappa = 2m_e(V_T - E)/\hbar^2$, where E is the energy of the state and z is the distance between the tip and sample surface. The tunneling current, J_T, is related to the tunneling probability and is proportional to Ψ^2.[17] Thus, $J_T \propto e^{\frac{-2z}{\hbar}\sqrt{2m_e(V_T - E)}}$. The sensitivity of an STM thus arises from the exponential dependence of the tunneling current on the distance between the tip and sample. In most cases, the terms of V_T and E are such that the magnitude of J_T decreases by an order of magnitude for a one angstrom increase in z.[17]

Scanning tunneling microscopy was widely adopted after it was used to solve the surface structure of the Si(111) 7x7 surface reconstruction.[18] STM is a powerful tool for the examination of surfaces and is capable of routinely obtaining atomically resolved images without interfering with surface processes.

Highly oriented pyrolytic graphite (HOPG) is a particularly useful surface for STM studies and it is frequently used as a calibration standard. A fresh atomically flat surface can be prepared simply by removing a layer from the HOPG sample using a piece of tape. Models and STM images of HOPG are shown in Figure 1.3. The quality of an STM image depends heavily upon the tip. Atomic resolution images of HOPG can readily be obtained using 80:20 Pt/Ir tips mechanically cut using scissors. Approximately 25–30% of tips prepared in this way yield STM images with resolution at the atomic scale. Of that number, only a few tips will yield an image as shown in Figure 1.3a; most of the 25–30% of tips that yield images with atomic resolution produce HOPG images, as shown in Figure 1.3c.

1.3 STM Imaging of Physisorbed Monolayers

The first images of molecules lying flat on a graphite surface were published in 1988 and were images of liquid crystals.[19] STM was soon used to image alkane monolayers on graphite.[20] The stable molecular monolayers proved to be an ideal sample for study by STM. Physisorbed monolayers can be imaged with an STM under ambient laboratory conditions, which vastly reduces the constraints related to sample handling and vibration isolation that are inherent to STM operation under the ultra high vacuum conditions used for many other STM studies.

STM has been used extensively in studies of physisorbed monolayers and numerous papers have been published on the topic.[21] Many of these studies have focused on the structure of the monolayers and the theory underlying the contrast observed in the images.[22–24] These issues were previously examined in the Lewis group by Christopher Claypool.[25–27] These particular studies consisted of a systematic investigation of the image contrast observed for functional groups such as halides, amines, ethers, thioethers, disulfides, carboxylic acids, double bonds, triple bonds, and nitriles. Theoretical techniques were then employed to compute STM images for sample molecules and the results of those computations were compared with the experimentally obtained STM images. Molecules were designed and synthesized such that functional groups which had appeared dark in contrast (such as bromide) were forced into a topographically different position, i.e., closer to the tunneling tip. The theoretically calculated images and the experimentally obtained images of these specially designed molecules underscored the fact that STM image contrast is a function both of the monolayer topography and of the electronic environment near functional groups.

STM images of physisorbed monolayers on graphite can be obtained under ambient laboratory conditions. A drop of a saturated filtered solution of the molecules of interest is placed on an HOPG sample such that the tip of the probe is wetted by the liquid. The solvent used is most commonly 1-phenyloctane, which possesses a low vapor pressure and does not form a monolayer of its own on the HOPG surface. Other solvents may be used provided that they are not electrically conductive. An image of an alkane monolayer on HOPG is shown in Figure 1.4. The molecules are aligned with their carbon skeletons parallel to the graphite surface. The image of the alkanes is actually that of the hydrogen atoms along the carbon chain which are topographically located closest to the tip as it is scanned over the surface. Individual hydrogen atoms are resolved in the image of a monolayer of *n*-tritriacontane shown in Figure 1.5. The relative positions of the hydrogen atoms indicate that the molecules lie on the surface with their carbon skeletons parallel to the surface.

Physisorbed monolayers cover the entire surface of an adsorbent such as HOPG. The two-dimensional monolayer structure is analogous to that of three-dimensional polycrystalline solids in that it is composed of multiple regions within which the two-dimensional unit cells are identically oriented. Each of these regions is called a domain and domains with differing unit cell orientations meet at regions termed domain boundaries. A single monolayer domain frequently covers the entire area of an STM image as shown in Figure 1.6. The monolayer structure is fluid and movement along domain boundaries can be captured in successive STM images, as shown in Figure 1.7. Studies of the movement within physisorbed monolayers and of the rates of exchange of molecules adsorbed to surface with those in the overlying liquid have been published.[28–30]

1.4 Summary

Many simple organic molecules spontaneously form highly ordered monolayers on surfaces. Early studies of this phenomenon were conducted using calorimetry and demonstrated that the intermolecular interactions dominated the driving force for monolayer formation. The invention of the scanning tunneling microscope provided an ideal tool for studying physisorbed monolayers and has allowed researchers to obtain images with resolution factors on the atomic scale.

Figure 1.1 Heat of Adsorption Versus Alkane Chain Length

This chart, from Ref. 1, shows the linear relationship between the length of straight-chain alkanes and the heat of adsorption of that alkane from an *n*-heptane solution onto a cast iron surface at 25°C.

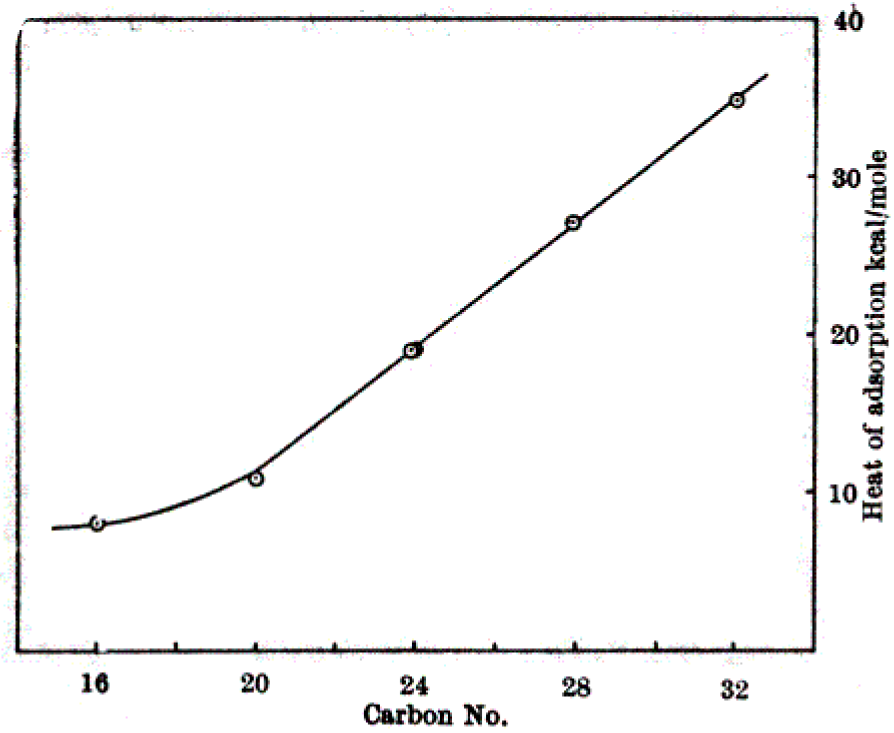

Figure 1.2 Diagram of a Scanning Tunneling Microscope

This diagram illustrates the operation of a scanning tunneling microscope during constant-current mode imaging and is adapted from Ref. 17. A sharp metal wire acts as the tip and is held at a constant voltage (V_T) relative to the sample. A stepper motor lowers the tip toward the sample until a current is detected. The x and y coordinate piezoelectric elements (P_X and P_Y) control the movement of the tip as it is scanned above the sample surface. The piezoelectric element P_Z controls the height of the tip above the sample (s), and the voltage controlling its position, V_P, is adjusted by feedback elements in the electronic control unit (CU) so that the tunneling current J_T is held at a constant value.

In this diagram, the tip travels from left to right and the vertical position of the tip is shown as a dotted line. The tip remains at a constant height about the sample until a surface step is reached at point A. The position of the tip is adjusted to maintain a constant J_T. A small amount of time is required to complete the height adjustment and during that time the tip is still being moved. This can result in a minor distortion of the apparent step width, δ. The sample surface possesses a region of lower work function at C. In order to maintain J_T, the position of the tip is adjusted (B). The resulting STM image is a map of the position of the tip as it is moved in a raster pattern across the surface and contains both topographic and electronic information about the sample.

Figure 1.2 Diagram of a Scanning Tunneling Microscope

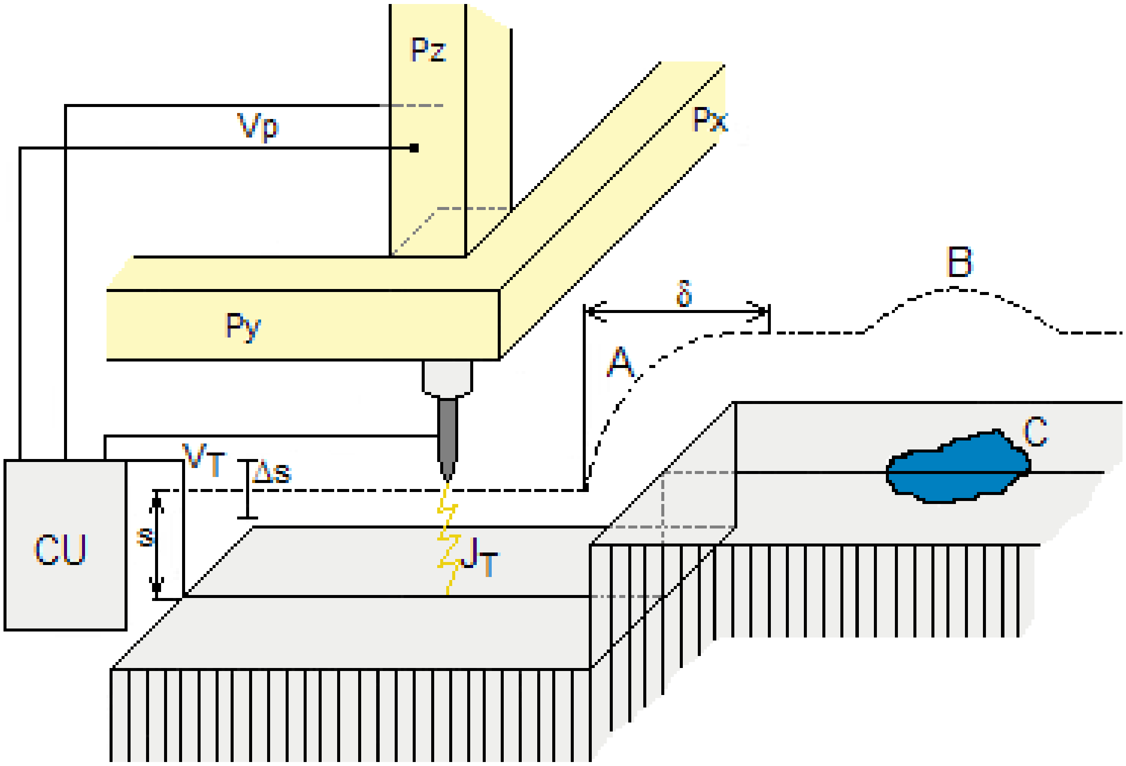

Figure 1.3 Models and STM Images of HOPG

(a) A constant height mode STM image of HOPG. The image exhibits atomic resolution and each carbon atom on the surface is visible. The hexagonal structure of the carbon atoms on the surface is highlighted in white. The deviation from a perfect hexagonal grid is due to thermal drift of the tunneling tip. Imaging conditions were 20 mV bias, 2 nA current, and a scan rate of 30.5 Hz.

(b) Models of the HOPG surface. The model on top shows the view along the direction normal to the surface. The atoms are separated by a distance of 1.42 Å. The model on the bottom shows the edge-on view which illustrates the layered structure of the solid. The distance between the layers is 3.34 Å.

(c) A typical STM image of HOPG. The image shows every other carbon atom on the surface. Imaging conditions are identical to those in (a).

(d) A model of the HOPG surface illustrating that the surface atoms are not equivalent. Half of the carbon atoms are positioned directly above atoms in the layer below. These atoms are highlighted in orange. The distance between the highlighted atoms is 2.46 Å.

Figure 1.3 Models and STM Images of HOPG

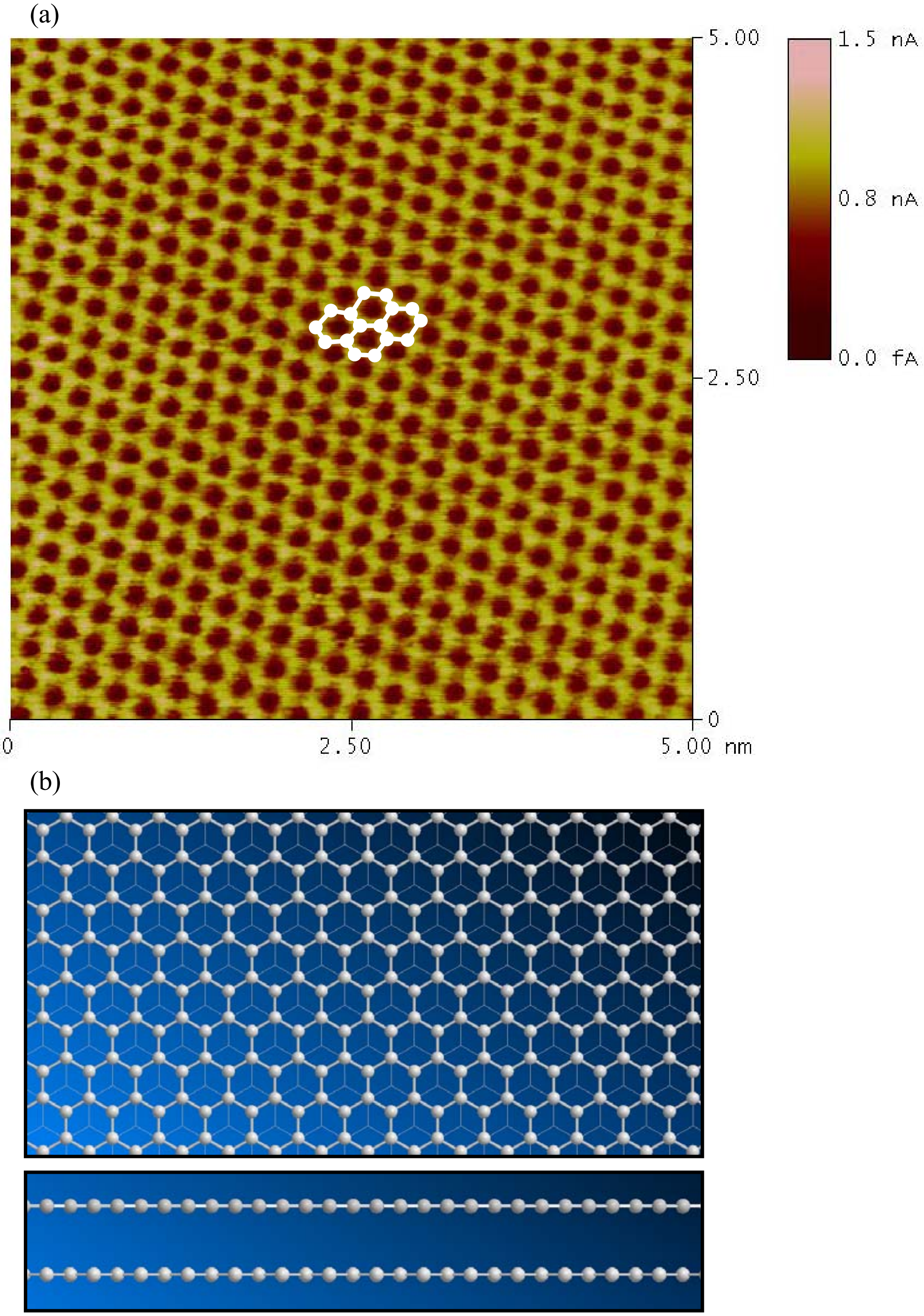

(c)

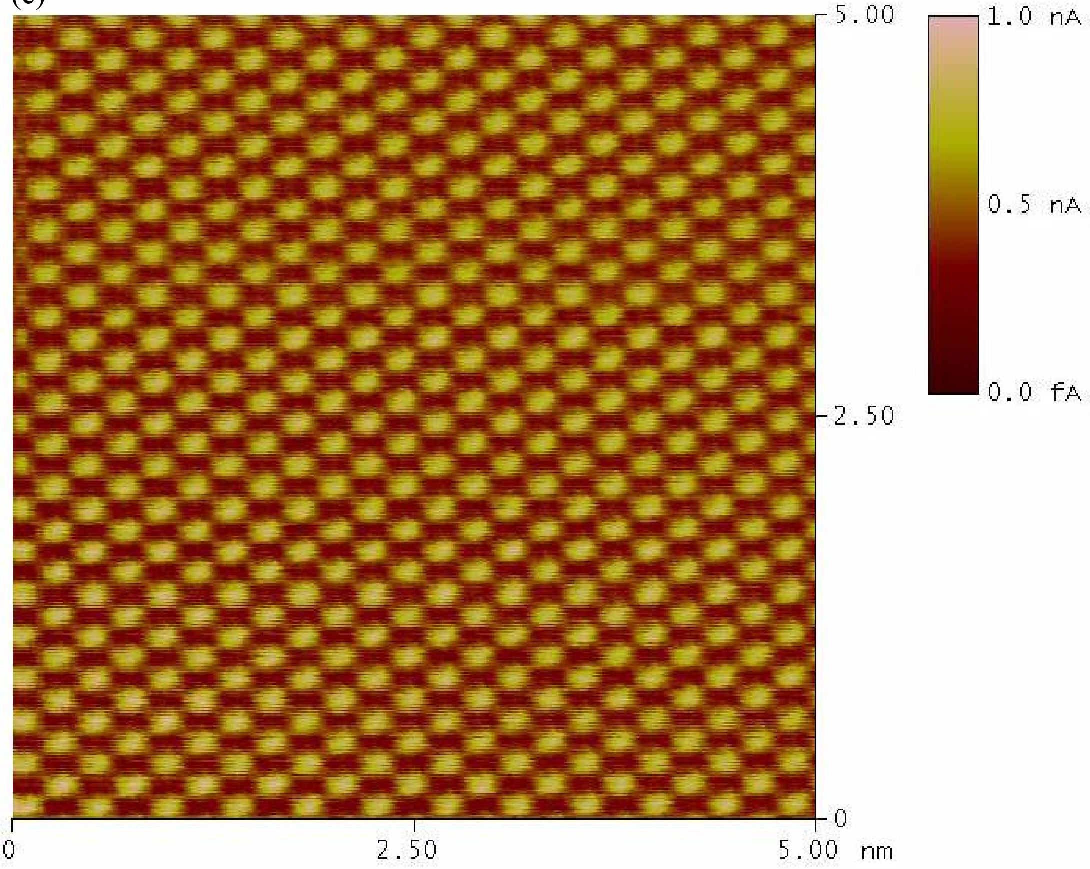

(d)

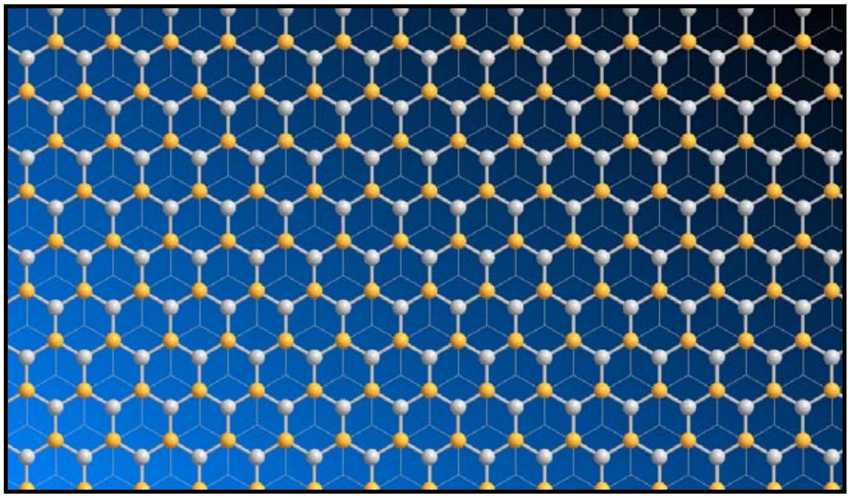

Figure 1.4 STM Image of Hexatriacontane on HOPG

A constant height mode STM image of a monolayer formed at the interface of HOPG and a solution of *n*-hexatriacontane, $CH_3(CH_2)_{34}CH_3$, in phenyloctane. Individual molecules are resolved in the image and several are highlighted by white lines. The imaging conditions were 1200 mV bias, 200 pA, and a scan rate of 30.5 Hz.

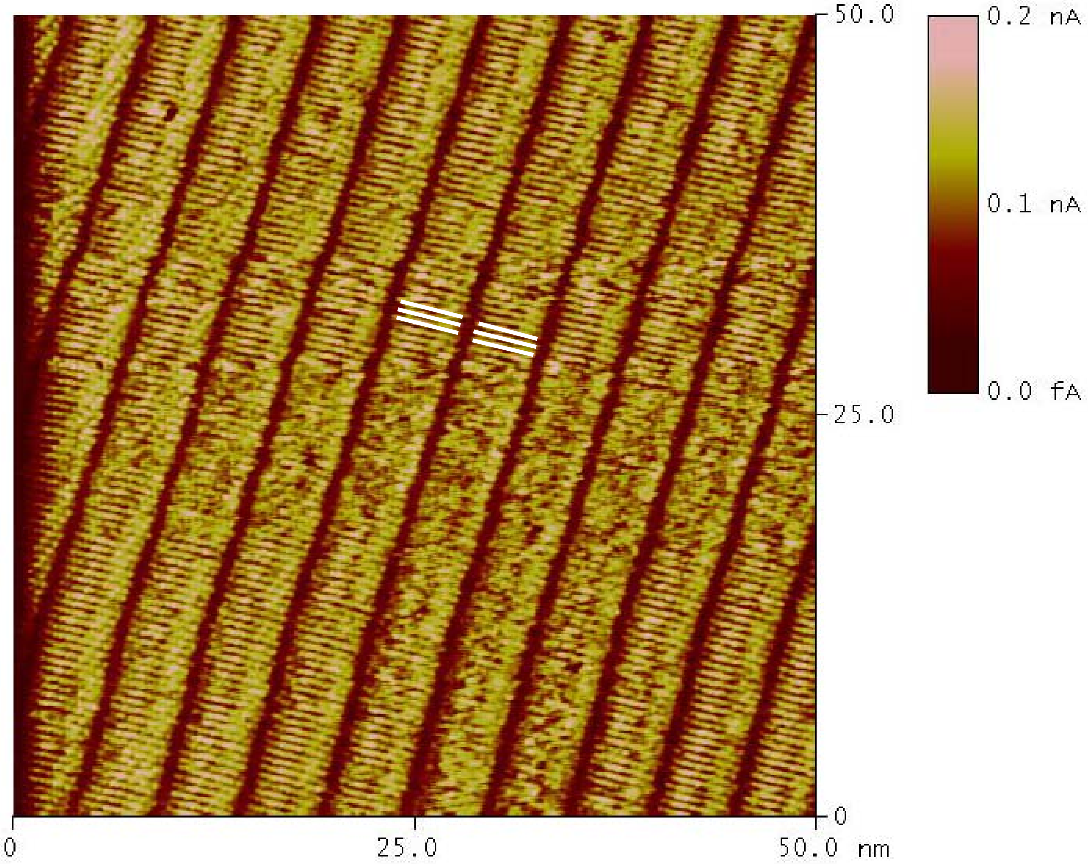

Figure 1.5 STM Image of Tritriacontane on HOPG

A constant height mode STM image of a monolayer formed on the surface of HOPG by a solution of *n*-tritriacontane, $CH_3(CH_2)_{31}CH_3$, in phenyloctane. The image of the molecule is that of the hydrogen atoms along the carbon backbone. The relative positions of the hydrogen atoms indicate that the molecules lie with their carbon skeletons parallel to the surface of the HOPG. One molecule is sketched in white, with the hydrogen atoms depicted as filled circles.

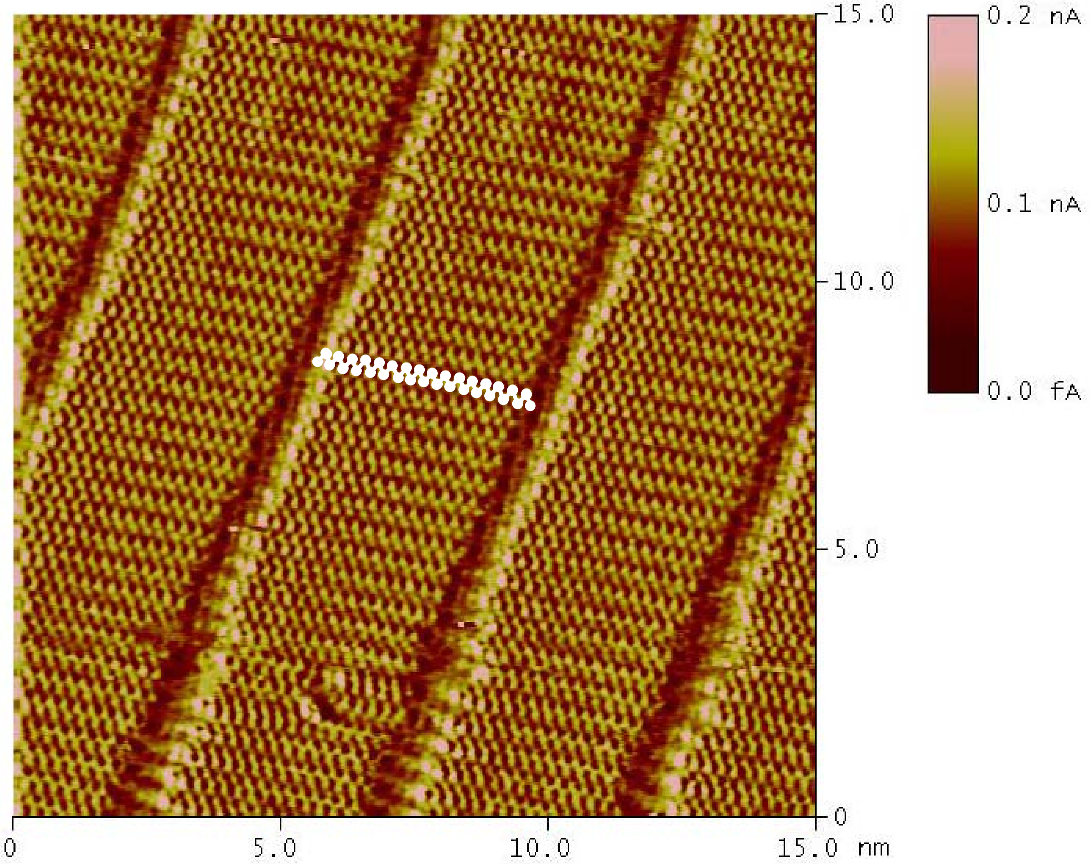

Figure 1.6 STM Image of 1-Tetradecanol on HOPG

A constant-current STM image of a monolayer formed at the interface of HOPG and a solution of 1-tetradecanol, $CH_3(CH_2)_{13}OH$, in phenyloctane. A single monolayer domain covers the entire image area. The molecules are arranged in a herringbone pattern with their oxygen atoms in the dark vertical stripes seen in the image. Imaging conditions were 1100 mV bias, 200 pA current, and scan rate of 30.5 Hz.

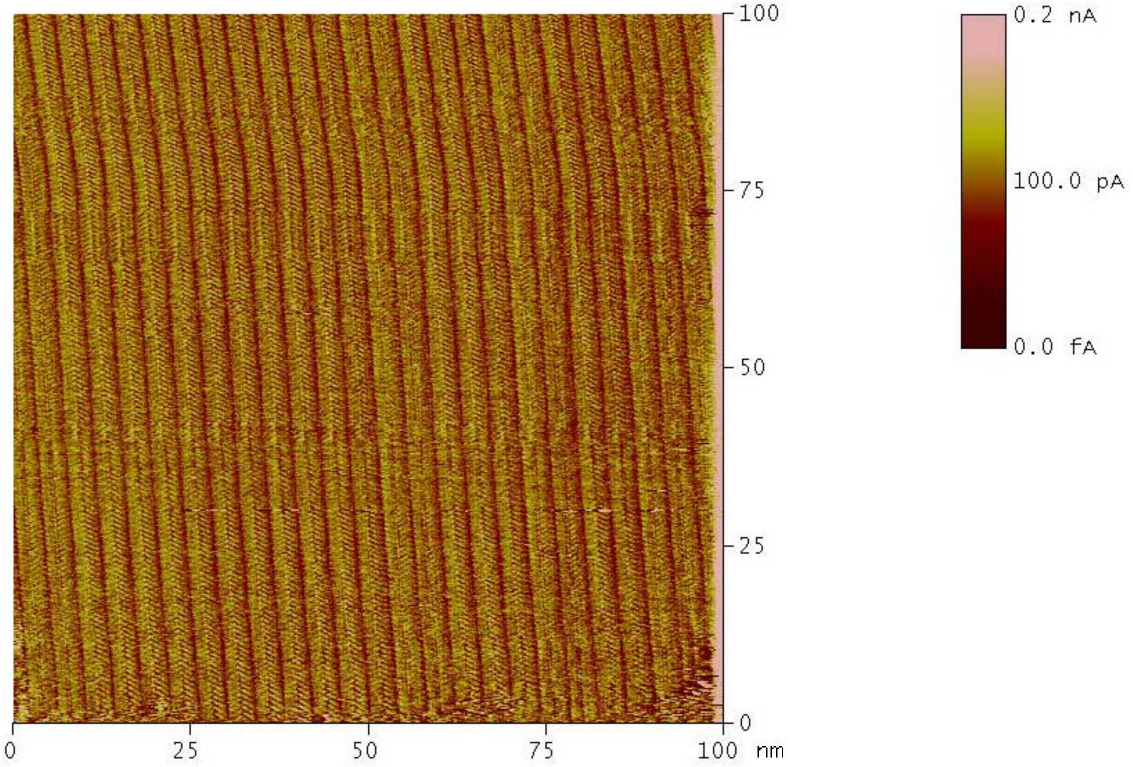

Figure 1.7 STM Images of Monolayer Domain Boundaries

Two constant height STM images of di-*n*-octadecylsulfide, $CH_3(CH_2)_{17}O(CH_2)_{17}CH_3$, in phenyloctane on HOPG. The images are of the same area of the surface and the time elapsed between them is two minutes. Domain boundaries are shown with white dashed lines. The position and number of boundaries change with time, illustrating the fluid nature of physisorbed monolayers. The imaging conditions were 1200 mV bias, 200 pA current, and a scan rate of 30.5 Hz.

Figure 1.7 STM Images of Monolayer Domain Boundaries

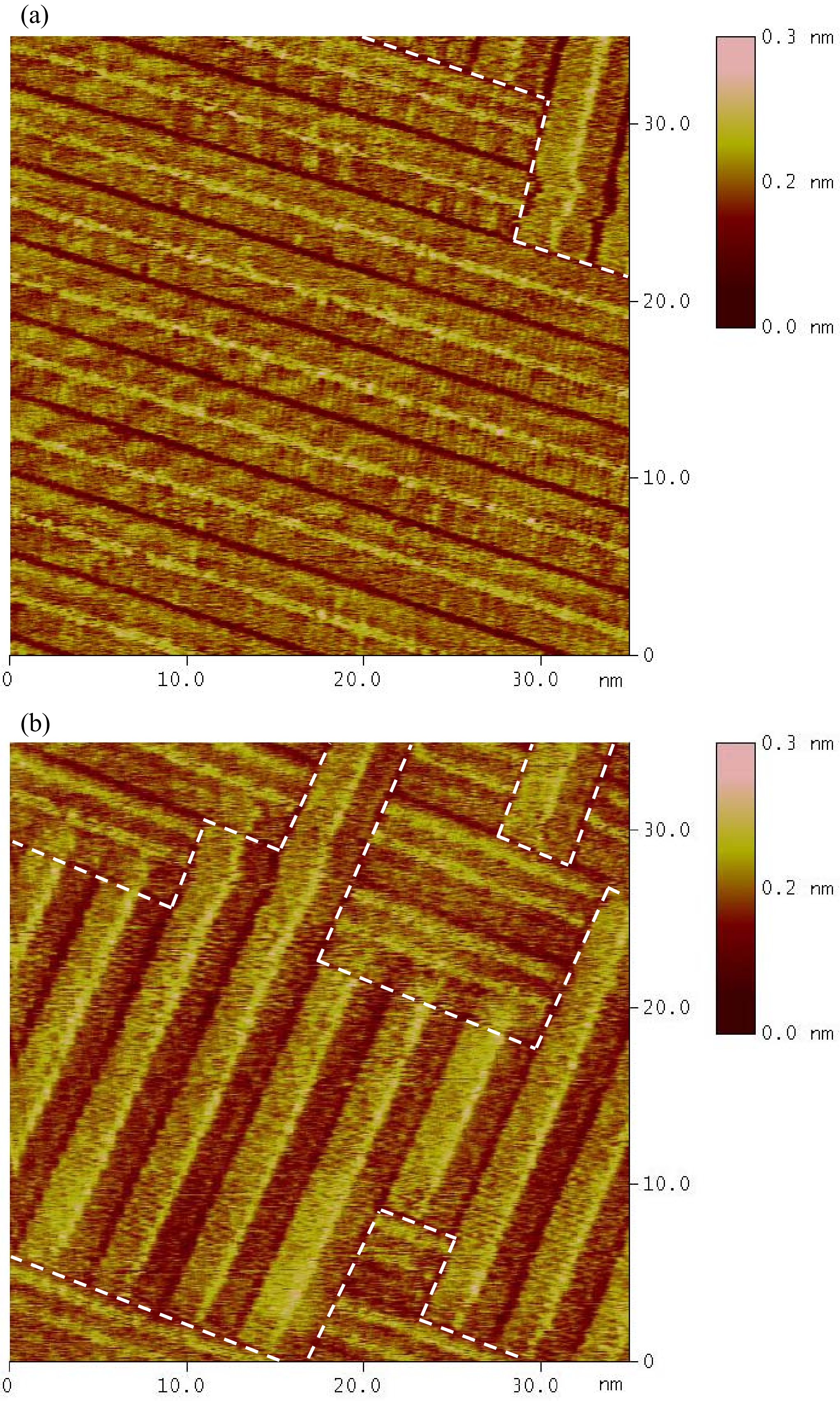

1.5 References

(1) Groszek, A. J. *Nature* **1962**, *196*, 531–533.

(2) Groszek, A. J. *Nature* **1964**, *204*, 680.

(3) Everett, D. H. *Transactions of the Faraday Society* **1965**, *61*, 2478–2495.

(4) Ash, S. G.; Everett, D. H.; Findenegg, G.H. *Transactions of the Faraday Society* **1968**, *64*, 2639–2644.

(5) Hentschke, R.; Winkler, R. G. *J. Chem. Phys*. **1993**, *99*, 5528–5534.

(6) Castro, M. A.; Clarke, S. M.; Inaba, A.; Dong, C. C.; Thomas, R. K. *J. Phys. Chem. B* **1998**, *102*, 777–781.

(7) Findenegg, G. H.; Liphard, M. *Carbon* **1987**, *25*, 119–128.

(8) Groszek, A. J. *Proceedings Of The Royal Society Of London Series A Mathematical And Physical Sciences* **1970,** 473–498.

(9) Florio, G. M.; Werblowsky, T. L.; Muller, T.; Berne, B. J.; Flynn, G. W. *J. Phys. Chem. B* **2005**, *109*, (10), 4520–4532.

(10) Kern, H. E.; Findenegg, G. H. *J. Colloid Interface Sci.* **1980**, *75*, 346–356.

(11) Fache, U.; Findenegg, G.H.; Kern, H.E.; Liphard, M. in *Microscopic Aspects of Adhesion and Lubrication*; Georges, J.M., Ed.; Elsevier: Amsterdam, 1982; pp 709–718.

(12) Herwig, K. W.; Matthies, B.; Taub, H. *Phys. Rev. Lett.* **1995**, *75*, 3154–3157.

(13) Ash, S. G.; Everett, D. H.; Findeneg, G.H. *Transactions of the Faraday Society* **1970**, *66*, 708–722.

(14) Binnig, G.; Rohrer, H. *Helvetica Physica Acta* **1982**, *55*, 726–735.

(15) Binnig, G.; Rohrer, H. *IBM Journal of Research and Development* **1986**, *30*, 355–369.

(16) Binnig, G.; Rohrer, H. *Angewandte Chemie—International Edition in English* **1987**, *26*, 606–614.

(17) *Methods of Experimental Physics Volume 27: Scanning Tunneling Microscopy*; Stroscio, J.A., Kaiser, W.J., Eds.; Academic Press: San Diego, 1993.

(18) Binnig, G.; Rohrer, H.; Salvan, F.; Gerber, C.; Baro, A. *Surf. Sci.* **1985**, *157*, L373–L378.

(19) Foster, J. S.; Frommer, J. E. *Nature* **1988**, *333*, 542–545.

(20) McGonigal, G. C.; Bernhardt, R. H.; Thomson, D. J. *Appl. Phys. Lett.* **1990**, *57*, 28–30.

(21) A wealth of literature on this topic has been published by the following authors: George W. Flynn of Columbia University; Jürgen P. Rabe of Humboldt Universität in Berlin; Frans C. De Schryver and Steven De Feyter at Katholieke Universiteit Leuven, Belgium; and Adam J. Matzger of the University of Michigan.

(22) Venkataraman, B.; Flynn, G. W.; Wilbur, J. L.; Folkers, J. P.; Whitesides, G. M. *J. Phys. Chem.* **1995**, *99*, 8684–8689.

(23) Xie, Z. X.; Xu, X.; Mao, B. W.; Tanaka, K. *Langmuir* **2002**, *18*, 3113–3116.

(24) Cousty, J.; Van, L.P. *Phys. Chem. Chem. Phys.* **2003**, *5*, 599–603.

(25) Faglioni, F.; Claypool, C. L.; Lewis, N. S.; Goddard, W. A. *J. Phys. Chem. B* **1997**, *101*, 5996–6020.

(26) Claypool, C. L.; Faglioni, F.; Matzger, A. J.; Goddard, W. A.; Lewis, N. S. *J. Phys. Chem. B* **1999**, *103*, 9690–9699.

(27) Claypool, C. L.; Faglioni, F.; Goddard, W. A.; Gray, H. B.; Lewis, N. S.; Marcus, R. A. *J. Phys. Chem. B* **1997**, *101*, 5978–5995.

(28) Padowitz, D. F.; Messmore, B. W. *J. Phys. Chem. B* **2000**, *104*, 9943–9946.

(29) Padowitz, D. F.; Sada, D. M.; Kemer, E. L.; Dougan, M. L.; Xue, W. A. *J. Phys. Chem. B* **2002**, *106*, 593–598.

(30) Muller, T.; Flynn, G. W.; Mathauser, A. T.; Teplyakov, A. V. *Langmuir* **2003**, *19*, 2812–2821.

(31) Claypool, C. L.; Faglioni, F.; Goddard, W. A.; Gray, H. B.; Lewis, N. S.; Marcus, R. A. *J. Phys. Chem. B* **1997**, *101*, 5978–5995.